PHILOSOPHICAL TRANSACTIONS OF THE ROYAL SOCIETY A MATHEMATICAL, PHYSICAL & ENGINEERING SCIENCES

On the role of ions in pulsed field ionization zero–kinetic–energy photoelectron spectroscopy

H. Palm, R. Signorell and F. Merkt

Phil. Trans. R. Soc. Lond. A 1997 **355**, 1551-1568
doi: 10.1098/rsta.1997.0076

On the role of ions in pulsed field ionization zero-kinetic-energy photoelectron spectroscopy

By H. Palm, R. Signorell and F. Merkt

Laboratorium für Physikalische Chemie, ETH-Zürich, CH-8092 Zürich, Switzerland

The high Rydberg states probed by pulsed field ionization (PFI) zero-kinetic-energy (ZEKE) photoelectron spectroscopy are usually produced simultaneously with ions. These ions can have a profound influence on the appearance of a ZEKE photoelectron spectrum. It is now widely accepted that ions can lead to a considerable stabilization of high Rydberg states with respect to internal decay processes such as predissociation and autoionization. Two further effects of ions on the outcome of a ZEKE photoelectron spectroscopic experiment are demonstrated: (1) high ionic concentrations can modify the response of atomic and molecular Rydberg state populations to pulsed electric fields; (2) high ionic concentrations can have a detrimental effect on the resolution of a ZEKE photoelectron spectrum. These effects are illustrated by experimental results, which include the determination of the structure of a *neutral* molecule, the ammonium radical, by PFI–ZEKE spectroscopy.

1. Introduction

The role of ions in pulsed field ionization experiments on high Rydberg states has been discussed in several recent articles (Chupka 1993; Pratt 1993; Zhang *et al.* 1993; Merkt 1994; Merkt & Zare 1994; Vrakking & Lee 1995*a*, *b*; Merkt *et al.* 1995, 1996; Vrakking *et al.* 1995; Jortner & Bixon 1995; Remacle & Levine 1996; Smith & Chupka 1995; Alt *et al.* 1995*a*, *b*). These articles have demonstrated, among other things, that ions produced in the same volume as high Rydberg states can lead to a considerable stabilization of the Rydberg states with respect to decay processes such as predissociation and autoionization.

The stabilization of high Rydberg states that is induced by the interaction with neighbouring ions is of relevance for new spectroscopic techniques such as pulsed-field ionization (PFI) zero-kinetic-energy (ZEKE) photoelectron spectroscopy which rely on the delayed (delay of typically 1 μs) pulsed field ionization of *long-lived* high atomic and molecular Rydberg states. In the absence of stabilizing processes induced by ions, several atomic and molecular systems undergo such rapid autoionization and/or predissociation processes that it is impossible to detect a delayed pulsed field ionization signal after delay times of several hundred nanoseconds. The Rydberg states converging on the upper spin-orbit threshold of argon ($Ar^+\ ^2P_{1/2}$), for instance, are so short lived that they can barely be observed (Weitzel & Güthe 1996) or cannot be observed at all (Hsu *et al.* 1996) in PFI–ZEKE experiments which use low fluence light sources such as synchrotrons, but can easily be detected when sources of higher spectral brightness are used (Merkt 1994; Muhlpfordt & Even 1995).

The effect of an ion on a Rydberg state located in its neighbourhood can be

Phil. Trans. R. Soc. Lond. A (1997) **355**, 1551–1568
Printed in Great Britain

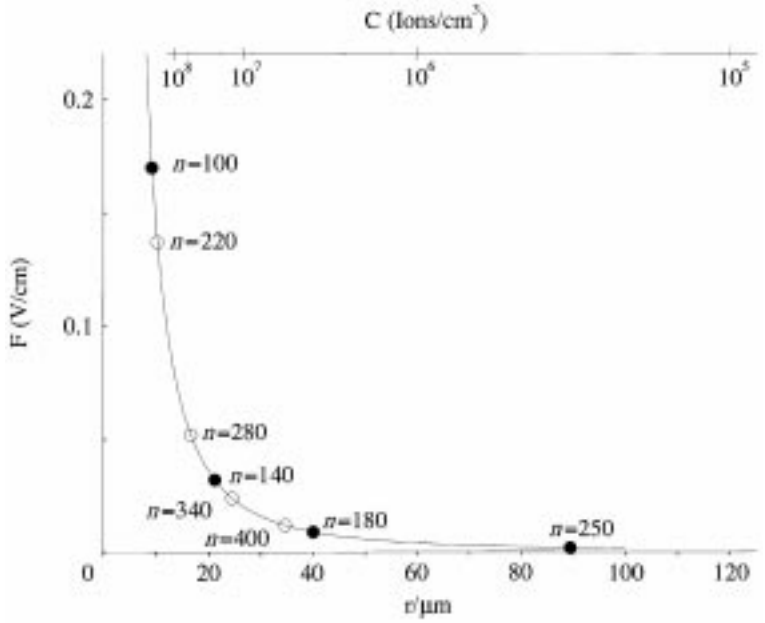

Figure 1. Effect of the field of an ion on high Rydberg states. The electric field of an ion is plotted against the distance from the positive charge centre. The open circles indicate the principal quantum numbers n above which the ionization of Rydberg states becomes classically allowed, and the full circles the n values above which a DC field of the magnitude indicated along the abcissa of the figure is expected to induce significant Stark-mixing in the Rydberg states. The upper horizontal scale indicates the ion concentrations at which the averaged field of the ionic distribution corresponds to the value given in the lower scale.

qualitatively understood by consideration of figure 1 which represents the electric field induced by the positive charge as a function of the distance r from the ionic centre. Also indicated on the figure are the principal quantum numbers n above which the ionization of Rydberg states becomes classically allowed, i.e. the n values (open circles) at which the Rydberg energy becomes larger than the saddle point in the electronic potential $V(r) = -1/r + Fz$ in atomic units, where the atomic unit of electric field is 5.1422×10^9 V cm^{-1}, and the n values (full circles) above which a DC field of the magnitude indicated along the abcissa of the figure is expected to induce significant Stark-mixing in the Rydberg states. The positions of the full circles are calculated from

$$F = 1/3n^5, \tag{1.1}$$

in atomic units, which characterizes the field at which the Rydberg-field interaction becomes comparable in magnitude with the spacing between H-atom Rydberg states of successive n values under field-free conditions (Merkt & Softley 1993; Gallagher 1994). The electric field of ions located 10 or 25 μm away from a molecule in Rydberg state n suffices to induce extensive Stark mixing above $n = 100$ or $n = 150$, respectively, and to cause their classical field ionization above $n = 220$ or $n = 350$, respectively.

The electric field of a distribution of ions is more difficult to evaluate than that of a single ion. In general, the fields of neighbouring ions tend to compensate each other and the electric field is not directly proportional to the ion concentration. Moreover, the field of a distribution of ions is strongly anisotropic and can induce

mixing between near-degenerate Stark states of different m-values (Merkt & Zare 1994) (m represents the magnetic quantum number). Holtsmark (1919) has derived an expression which relates ion concentrations to the electric field distribution in space. In particular, he obtained

$$\bar{F} = 3.75 \times 10^{-7} C^{2/3}, \tag{1.2}$$

which relates the absolute value $\bar{F}$ (in V cm^{-1}) of the electric field averaged over space to the ion concentration C (in ions cm^{-3}). In a PFI–ZEKE experiment, some Rydberg states are exposed to fields significantly larger, others to fields significantly weaker than predicted by equation (1.2). Nevertheless, this equation is useful to obtain a rough estimate of the concentrations at which neighbouring ions can be expected to influence the properties of high Rydberg states. Conversely, a rough estimate of the ion concentration may be obtained, via equation (1.2), from the analysis of the pulsed field ionization behaviour of high Rydberg states, as is shown below.

The ion concentrations which lead, according to equation (1.2), to the fields $\bar{F}$ given along the abcissa in figure 1 are indicated on the horizontal scale at the top of the figure. At ion concentrations of $C = 10^4$, 10^5, 10^6, 10^7 and 10^8 ions cm^{-3}, $\bar{F}$ takes values of 0.2, 1, 4, 20 and 80 mV cm^{-1}, respectively. A homogeneous electric field of the same magnitude would induce significant Stark mixing in Rydberg states with n values above 355, 255, 190, 135 and 100, respectively.

Whether a given ion concentration contributes to modification of the physical behaviour of high Rydberg states, such as their lifetimes or their field ionization behaviour, depends on additional experimental factors as follows.

(i) The choice of the magnitude and shape of the pulsed field used to field ionize the Rydberg states determines the range of n values probed in the experiment, and thus determines whether the states probed are sensitive to the fields induced by neighbouring ions. In its high resolution version, PFI–ZEKE spectroscopy probes Rydberg states with $n > 250$. Ion concentrations as low as 10^4 to 10^5 ions cm^{-3} can still have an influence on the properties of these states (see figure 1).

(ii) Carrying out pulsed field ionization experiments on high Rydberg states in the presence of a homogeneous electric field reduces the effects of ions. In the presence of a homogeneous DC electric field of 20 mV cm^{-1}, for instance, the average field $\bar{F}$ of an ionic distribution is likely to be negligible at concentrations below 10^6 ions cm^{-3}. That a homogeneous electric field reduces the effects of ions on a Rydberg state population has been demonstrated experimentally (Merkt 1994) and in model calculations (Merkt & Zare 1994).

If the effects of ions on high Rydberg states are such that their decay is slowed down by several orders of magnitude, it may be possible to study these effects by investigating properties of high Rydberg states other than their lifetimes. In the course of the research presented in this contribution and elsewhere (Signorell *et al.* 1997; Palm & Merkt 1997), we have demonstrated: (1) that the dominant effect of ions on high Rydberg states is to induce mixing among near-degenerate Stark states; (2) that this mixing can be probed with high sensitivity by analysing the field ionization behaviour of the Rydberg state population by sequences of electric field pulses of equal magnitude; and (3) that high ionic concentrations $c > 10^6$ ions cm^{-3} have a detrimental effect on the resolution that can be achieved by PFI–ZEKE or MATI (mass-analysed threshold ionization) spectroscopies.

In our experiments with electric field sequences, we notice that ion concentration

effects on the pulsed field ionization behaviour of high Rydberg states with principal quantum number in the range $100 < n < 350$ are dominant at concentrations $c > 10^6$ ions cm^{-3}, decrease in importance in the range 10^6–10^4 ions cm^{-3} and are not detectable at a concentration $c < 10^4$ ions cm^{-3}. At such low ion concentrations the measurement of PFI–ZEKE photoelectron spectra with a resolution significantly better than 1 cm^{-1} becomes possible as is illustrated here with the example of the ZEKE spectrum of the nitric oxide and the ammonium radicals.

2. Experiment

The experimental setup, which consists of a laser system and a linear electron–ion time-of-flight spectrometer, has been presented elsewhere (Signorell *et al.* 1997) and only a short description is given here. The laser system consists of two Nd:YAG-pumped dye lasers. The output of both dye lasers can be scanned in the range $\lambda = 200$–760 nm by using appropriate doubling and mixing crystals. An optical delay line can be used to delay one laser up to 100 ns with respect to the other. Both dye laser beams are recombined with a dichroic mirror and propagated collinearly into the photoionization region where they cross a skimmed supersonic expansion of the sample gas at right angles in the middle of a 5.7 cm long stack of extraction plates designed for the application of homogeneous pulsed and DC electric fields. Pulsed fields ranging from a few mV cm^{-1} to 900 V cm^{-1} can be applied across the stack of extraction plates with a rise time of 50 ns. In the range 0–1.5 V cm^{-1}, an arbitrary function generator can be used to generate pulsed fields of any desired form.

The sample gas is directed in a skimmed supersonic expansion toward the multichannel plate detector (in chevron configuration) which enables the recording of photoionization spectra with ion extraction fields of less than 1 V cm^{-1}. The extraction and time-of-flight regions are surrounded by a double magnetic shield. Estimated stray fields amount to less than 10 mV cm^{-1}. In the experiments on NO, only one dye laser is used in the range 37 000–38 000 cm^{-1}. In the experiments on ND_4, the first dye laser ($\lambda_1 \approx 200$ nm) precedes the second dye laser (λ_2 =260–280 nm) by 28 ns.

3. Photoionization and PFI–ZEKE experiments on NO

Figure 2 shows two PFI–ZEKE spectra (traces (*a*) and (*b*)) and a photoionization spectrum (trace (*c*)) of NO in the region of the $X\ ^1\Sigma^+(v^+ = 0) \leftarrow X\ ^2\Pi_{1/2}(v = 0)$ photoelectronic transition. The spectra were obtained following non-resonant two-photon absorption from the ground state. The assignment of the ZEKE spectrum is indicated on the figure in terms of the total angular momentum quantum number J'' of the rotational levels of the ground state (at the right of the assignment bars) and the rotational angular momentum quantum number N^+ of the ion (below the assignment bars). The assignment of the photoionization spectrum is also given in figure 2. The spectrum was obtained by extracting the ions with a DC electric field of 1.75 V cm^{-1}. Trace (*c*) in figure 2 shows that the total ion concentration produced in the photoexcitation volume strongly depends on the two-photon wavenumber. This observation shows that ion concentrations in PFI–ZEKE experiments are difficult to control. They are not solely determined by the laser fluence but also by the wavenumber dependence of the photoionization cross section. This wavenumber dependence makes it in general impossible to characterize ion concentrations by a

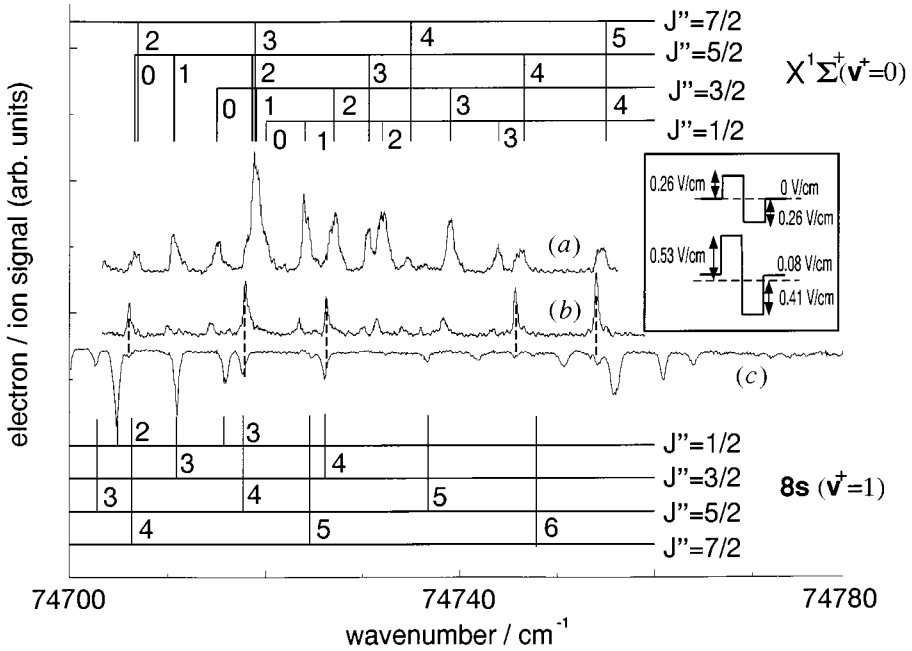

Figure 2. PFI–ZEKE photoelectron (traces (*a*) and (*b*)) and photoionization (trace (*c*)) spectra of NO recorded following two-photon non-resonant absorption from the ground state. The numbers in the body of the figure are the quantum numbers N^+ of the rotational levels of the ion.

single number: ion concentrations can vary over several orders of magnitude over small wavenumber ranges. With the laser pulse energies (800 μJ pulse^{-1}) and focusing conditions (spherical lens with focal length of 16 cm) used for the recording of the spectra in figure 2, the total ion concentration varied between approximately 5×10^4 and approximately 10^7 ions cm^{-3} over the wavenumber range of the figure.

The pulse sequences used to record the PFI–ZEKE spectra are indicated as inserts above the corresponding traces. They consist of a positive discrimination field used to sweep unwanted electrons out of the excitation region and to prevent the detection of the highest Rydberg states (which has the effect of improving the resolution (Palm & Merkt 1997; Dietrich *et al.* 1996)), immediately followed by a second negative field. The spectra are obtained by monitoring the yield of electrons produced by this second field as a function of the two-photon wavenumber. The Rydberg states that give rise to the PFI–ZEKE spectrum displayed in the middle trace of figure 2 are located energetically below those probed by the field sequence used to record the upper trace (trace (*a*)). An appropriate choice of pulsed field sequences can thus be used to probe Rydberg states located in well-defined energy windows below an ionization threshold.

The intensities of the rotational lines in traces (*a*) and (*b*) are very different. Some of the most intense lines in trace (*b*), such as for instance the transitions $J'' = \frac{5}{2} \rightarrow N^+ = 0$, $J'' = \frac{5}{2} \rightarrow N^+ = 4$ and $J'' = \frac{3}{2} \rightarrow N^+ = 4$, are weak in trace (*a*). The origin of the intensities of the particularly strong lines in trace (*b*) becomes obvious when one compares their positions with the positions of the autoionization resonances in the photoionization spectrum (trace (*c*) in figure 2). At the position of each strong line in the PFI–ZEKE spectrum displayed in trace (*b*), an autoionization resonance is observed in the photoionization spectrum, the correspondence being

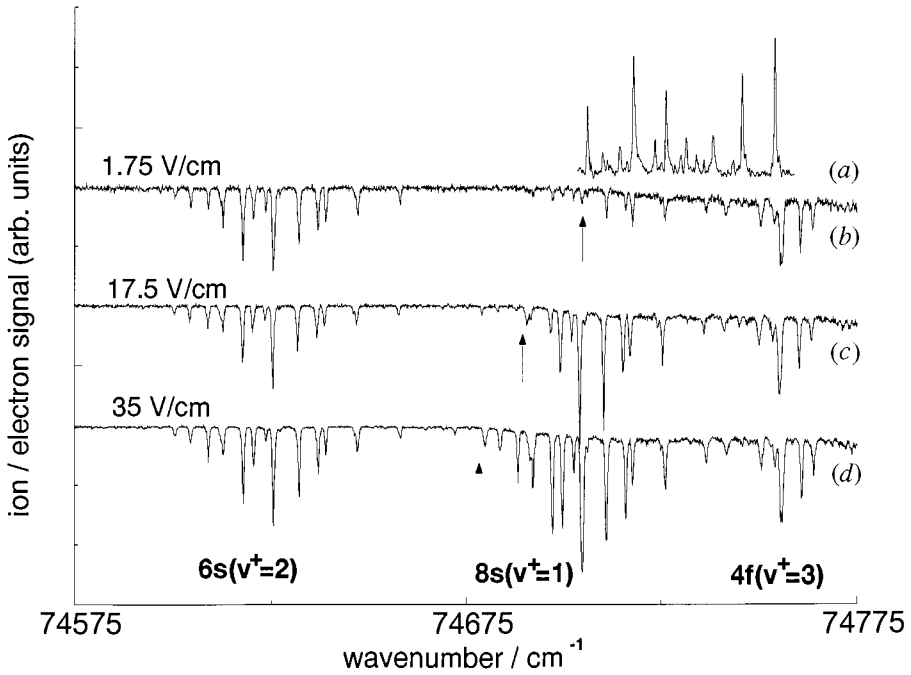

Figure 3. Photoionization spectra of NO in the vicinity of the first ionization limit. DC electric fields of 1.75, 17.5 and 35 V cm^{-1} have been used to record traces (b)–(d). Trace (a) represents the ZEKE photoelectron spectrum of NO.

indicated by dashed vertical lines in the figure. The channel interactions responsible for the observation of the autoionization resonances in the photoionization spectrum also give rise to intensity enhancements in the PFI–ZEKE spectrum in trace (b). Trace (a) is less affected by these channel interactions than trace (b) because the Rydberg states probed by the pulsed field ionization sequence lie on the high-energy side of the autoionization resonances. Figure 2 thus provides a clear illustration of the importance of channel interactions on line intensities in PFI–ZEKE spectroscopy (see Merkt & Softley (1993, 1992a, b) for other examples). Because of the sharp nature of the autoionizing resonances in NO, the intensity distributions in the PFI–ZEKE spectra are extremely sensitive to the position of the energetic window probed by the pulse sequence.

Figure 3 shows photoionization spectra of NO that were recorded in the vicinity of the lowest ($v^+ = 0$) ionization thresholds following non-resonant two-photon absorption from the ground state. The ionization signals in traces (b)–(d) were obtained by extracting the ions with DC fields of 1.75, 17.5 and 35 V cm^{-1}, respectively. The ZEKE spectrum of the $^1\Sigma(v^+ = 0) \leftarrow X\ ^2\Pi_{1/2}(v = 0)$ band obtained with a pulsed field of -410 mV cm^{-1} preceeded by a discrimination pulse of $+530$ mV cm^{-1} is represented in trace (a) and indicates the position of the ionization thresholds. The onset of ionization is also visible in the photoionization spectra as an increase in the baseline indicated by vertical arrows. The increasing DC fields used to extract the NO^+ ions lead to a shift of this onset toward lower wavenumbers because the ionization limits are lowered by the DC field.

Sharp structures are superimposed on the smoothly varying photoionization background which can be classified in three groups of photoionization lines. The first group

of lines is located well below the ZEKE spectrum between 74 670 and 74 720 cm^{-1} and was assigned, on the basis of the work of Miescher (1976) and Miescher & Huber (1976) to the (2 + 1) resonance-enhanced multiphoton ionization (REMPI) of the 6s ($v^+ = 2$) $\leftarrow X\ ^2\Pi^+_{1/2}(v = 0)$ transition. The second group of lines in the range 74 670–74 720 cm^{-1}, corresponding to the 8s ($v^+ = 1$) $\leftarrow X\ ^2\Pi^+_{1/2}(v = 0)$ two-photon transition, is located in the same spectral region as the high Rydberg states converging on the first rotational levels of the ground vibronic state of the ion. The assignment of the rotational structure of this band is given in figure 2. The third group of lines (assigned to the 4f ($v^+ = 3$) $\leftarrow X\ ^2\Pi^+_{1/2}(v = 0)$ transition (Jungen & Miescher 1969)) is located above the ionization thresholds (Reiser *et al.* 1988) around 74 750 cm^{-1}.

Whereas the relative intensities of the transitions in the first and third groups of lines are the same regardless of the magnitude of the DC fields used to extract the ions, the intensities of the lines in the second group increase rapidly with increasing DC field. This behaviour is not easy to interpret and has its origin in competing processes. Forced autoionization to the $v^+ = 0$ continuum can be invoked to explain the presence of the strong lines in traces (*c*) and (*d*) and their absence in trace (*b*): the corresponding states, which are coupled to the $v^+ = 0$ channels, but are located below the field free $v^+ = 0$ ionization thresholds, can only autoionize when the magnitude of the DC field lowers the ($v^+ = 0$) ionization thresholds. The fact that the lines are observed on the high frequency side of the arrows indicating the onset of ionization in traces (*b*)–(*d*) supports this interpretation: the ionization mechanism for the 8s ($v^+ = 1$) Rydberg states in traces (*c*) and (*d*) appears to be forced autoionization rather than (2 + 1) REMPI.

This interpretation is however not fully satisfactory: (2 + 1) REMPI, which leads to strong ionization signals between 74 550 and 74 650 cm^{-1} ought also to cause the ionization of the states located in the range 74 670 and 74 720 cm^{-1}. *The reduced intensity of the second group of lines in trace (b) thus also requires an explanation.* A possible interpretation is that the coupling between the low-n states and the high Stark-mixed Rydberg states located below the $v^+ = 0$ limit inhibits the probability of absorption of a third photon and weakens (2 + 1) REMPI ionization signals. An additional complication in the determination of ion concentration in PFI–ZEKE experiments results: the total ion concentration at a given wavenumber also depends on the DC electric field present at the time of photoexcitation; it is significantly higher in the region of the PFI–ZEKE spectrum under the conditions of traces (*c*) and (*d*) than under the conditions of trace (*b*).

4. Effects of ion concentrations on PFI and ZEKE spectra

To investigate the role of ion concentrations on the PFI behaviour of high Rydberg states of NO, we use sequences of pulsed electric fields of equal magnitude such as those displayed in figures 4 and 5 which also show the PFI signal above the electric field pulse sequence. The usefulness of these pulse sequences, first used in reference (Merkt *et al.* 1996), originates from the fact that an ionization signal observed from any pulsed field after the first unambiguously betrays a change in the character of the Rydberg states that has taken place in the interval separating successive pulses. This change must be such that it converts a Stark state from a state that resisted ionization by all previous pulsed fields to a state that can ionize by an *identical* pulsed field. The conversion may follow from a change of k (equal to $n_2 - n_1$, where

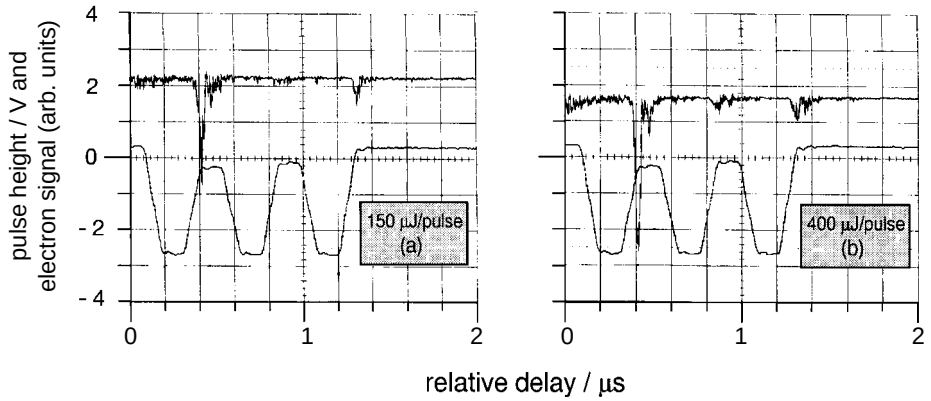

Figure 4. Pulsed field ionization of $n \approx 200$ Rydberg states of NO with sequences of pulsed electric fields of equal amplitudes. Panels (a) and (b) show the electric field sequences and the pulsed field ionization signals obtained when NO is photoexcited with light pulses of 150 and 400 μJ average pulse energy, respectively.

n_1 and n_2 represent the parabolic quantum numbers that arise in the solution of the Schrödinger equation of the H-atom in parabolic coordinates (Bethe & Salpeter 1957)), of m, or of n (Merkt *et al.* 1996; Palm & Merkt 1997).

The electric field sequences used to obtain the pulsed field ionization signals in figures 4 and 5 are such that the electric field is brought back to zero between the last two pulses but to a small non-zero field between the first two pulses. Panels (a) and (b) in figure 4 show two measurements with sequences of three pulsed fields in which the electric field was brought back from $-440\,\mathrm{mV\,cm^{-1}}$ to $-25\,\mathrm{mV\,cm^{-1}}$ between the first two pulses and to $0\,\mathrm{mV\,cm^{-1}}$ between the last two pulses. Photoexcitation was carried out with light pulses of 150 and 400 μJ energy, respectively. A 15 cm focal length spherical lens was used to drive the two-photon absorption to $n \approx 200$ high Rydberg states of NO resulting in ion concentrations of 10^6–10^7 ions $\mathrm{cm^{-3}}$ in the measurement shown in panel (b) and of concentrations 5–10 times smaller for panel (a). The fact that the third pulsed field induces a PFI signal in panel (a), but the second does not, demonstrates that the condition for the observation of recurrent PFI signal is that the electric field returns sufficiently close to zero between successive pulses.

At the high fluences and ion concentrations used for obtaining panel (b), the $-25\,\mathrm{mV\,cm^{-1}}$ field maintained between the first two pulses is insufficient to inhibit the field ionization by the second pulsed field. The figure thus shows that the k, m or n changes that lead to the second PFI signal in panel (b) are a consequence of the increased ion concentration compared to panel (a). The interaction between the Rydberg states and neighbouring ions thus modifies the pulsed field ionization behaviour of the Rydberg states.

Figures 5a, b show two sets of PFI measurements carried out at laser energies of 400 and 90 μJ $\mathrm{pulse^{-1}}$, respectively. The magnitude of the electric field maintained between the first two pulses amounts to 0, 23 and 45 $\mathrm{mV\,cm^{-1}}$ for the upper, middle and lower panels of figure 5a and to 0, 11 and 23 $\mathrm{mV\,cm^{-1}}$ for the corresponding panels in figure 5b. Whereas a field $|F| > 11\,\mathrm{mV\,cm^{-1}}$ suffices to inhibit recurrent field ionization at the ion concentrations 10^5–10^6 ions $\mathrm{cm^{-3}}$ in figure 5b, a field $|F| > 23\,\mathrm{mV\,cm^{-1}}$ is required at the higher ion concentrations of 10^6–10^7 ions $\mathrm{cm^{-3}}$ in figure 5a.

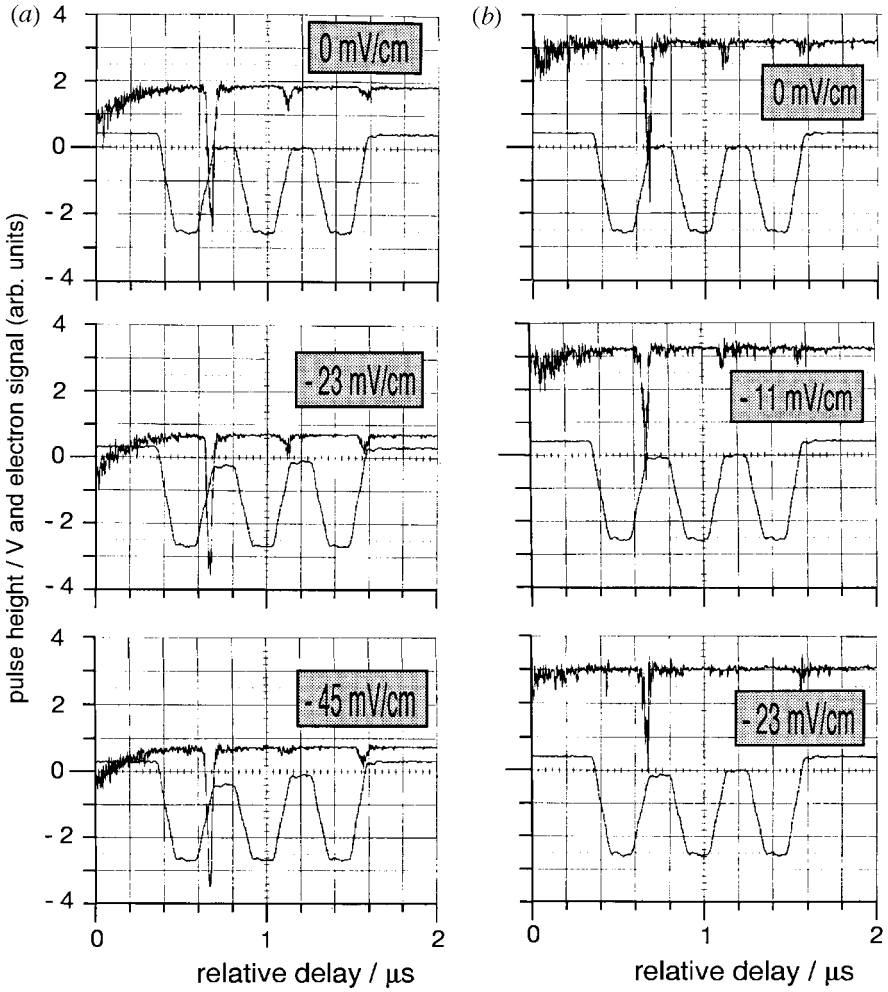

Figure 5. Pulsed field ionization of $n \approx 200$ Rydberg states of NO with sequences of pulsed electric fields of equal amplitudes. The electric field returns to zero between the pulsed fields in the top panels of (*a*) and (*b*) which correspond to measurements made at pulse energies of 400 μJ pulse^{-1} and 90 μJ, respectively. An electric field of −23 or −45 mV cm^{-1} is maintained in the interval separating the first two pulsed fields in the middle or bottom panel of (*a*), respectively. For the corresponding traces in (*b*) these fields amount to −11 or −23 mV cm^{-1}, respectively.

It is interesting to note that the −23 mV cm^{-1} DC field maintained between the first two pulses in the lower panel of figure 5*b* and in the middle panel in figure 5*a* is significantly greater than the values of $\bar{F}$ predicted with equation (1.2) for ion concentrations of 10^5–10^6 ions cm^{-3} (corresponding to experimental conditions of figure 5*b*), but comparable to $\bar{F}$ at ion concentrations 10^6–10^7 ions cm^{-3} (corresponding to the experimental conditions of figure 5*a*). *Recurrent field ionization is inhibited when the homogeneous DC field maintained between successive pulses exceeds the value of the (inhomogeneous) field of the ionic distribution. A correlation thus exists between* $\bar{F}$ *(see equation (1.2)) and the magnitude of the field required to inhibit a recurrent field ionization.* This correlation may be useful to obtain a rough estimate of ion concentrations in PFI experiments.

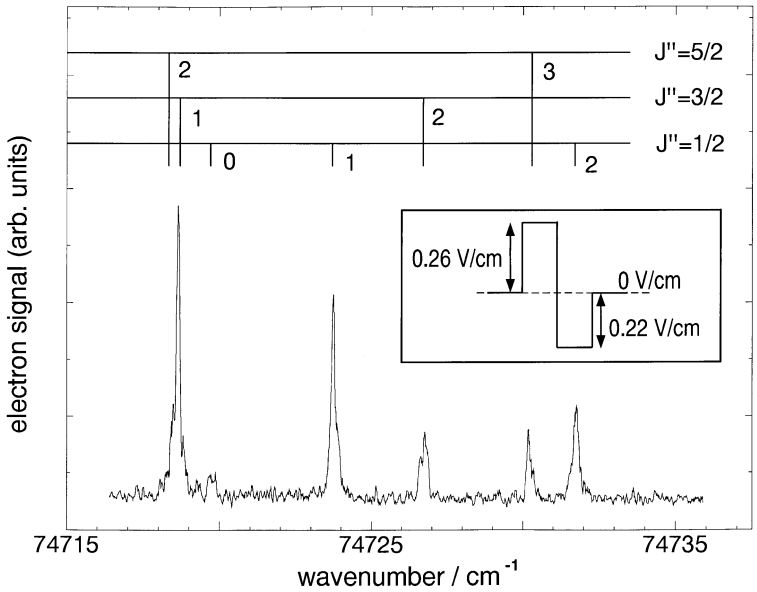

Figure 6. High resolution PFI–ZEKE photoelectron spectrum of NO in the region of the first ionization limit.

At ion concentrations $C \leqslant 10^4$ ions cm^{-3}, no recurrent field ionization signal in the range $n < 350$ could be detected, within the limits of our sensitivity, with pulsed field sequences such as those used in figures 4 and 5. Under conditions where ion concentrations have been minimized, the resolution that can be achieved in PFI–ZEKE experiments can be markedly improved, as is illustrated in figure 6 which represents a portion of the two-photon non-resonant PFI–ZEKE spectrum of NO recorded with a pulsed field sequence consisting of a discrimination pulse of +260 mV cm^{-1} immediately followed by a second field of −220 mV cm^{-1}. The peaks in figure 6 have FWHM ranging from 0.15–0.25 cm^{-1}. The resolution is comparable with the 0.2 cm^{-1} resolution reported by Dietrich *et al.* (1996) and represents the highest resolution obtained to date by PFI–ZEKE spectroscopy.

5. High resolution PFI–ZEKE spectroscopy of the ammonium radical

In this section, the rotationally resolved photoelectron spectrum of the ammonium radical serves to illustrate the power of high-resolution PFI–ZEKE spectroscopy under conditions where the ion concentrations have been minimized. The ammonium radical is a molecule for which only very restricted information is available. The molecule only exists in metastable Rydberg states. It consists of an NH_4^+ ion core surrounded by a Rydberg electron. The lowest electronic state is a state where the Rydberg electron occupies a 3s a_1 Rydberg orbital outside the NH_4^+ closed-shell configuration $[(1a_1)^2(2a_1)^2(1f_2)^6]$. Only one progression of bands, the so-called Schüler band system, has been observed for this molecule (Herzberg 1981; Schüler *et al.* 1955; Alberti *et al.* 1984; Huber & Sears 1985; Whittaker *et al.* 1984). The main Schüler band has been assigned by Alberti *et al.* (1984) to the transition between the vibrationless upper 3p $^2F_2$ and lower 3s $^2A_1$ states of NH_4. Other weaker bands of the Schüler system have been analysed by Watson (1986).

Unfortunately, because the main Schüler band is a $^2F_2$–$^2A_1$ transition, and because

no combination differences can be derived from such a transition in molecules of tetrahedral geometry, only differences between the rotational constants of the $^2F_2$ and the $^2A_1$ states can be extracted from a fit of the rotational structure of the Schüler band (Alberti *et al.* 1984). The structure of the ammonium radical can thus not be derived from allowed single-photon absorption and emision bands. Measuring the high resolution photoelectron spectrum of the transition between the 3s $^2A_1$ state of the ammonium radical and the ground $\tilde{X}\ ^1A_1$ state of the ammonium ion makes it possible to overcome this restriction. Combination differences, and hence rotational constants, for both states involved in an allowed A_1–A_1 photoelectronic transition can be derived from the analysis of the rotational structure of the spectrum. It is only since the completed analysis of the rotational structure of the high-resolution PFI–ZEKE spectrum that precise spectroscopic and structural information exists on the ammonium radical (Signorell *et al.* 1997).

Spectroscopic experiments on the ammonium radical are complicated by the fact that the lowest bound state (the 3s $^2A_1$ state) is very short lived for all isotopomers apart from ND_4 which has a lifetime of several microseconds (Williams & Porter 1980). For this reason we chose to investigate this isotopomer by high resolution PFI–ZEKE photoelectron spectroscopy.

The ammonium radicals are produced in two steps, the formation of $(ND_3)_n$ clusters in a skimmed supersonic expansion followed by the photodissociation of these clusters with laser pulses in the wavelength range around 200 nm, a wavelength range enabling photoexcitation to the cluster analogues of the dissociative $\tilde{A}$ state of ammonia.

The degree of clustering in our experimental setup critically depends on the nozzle backing pressure and gas mixture. When pure ND_3 is expanded at a backing pressure of 6 bar, and the $(ND_3)_n$ cluster distribution is probed mass spectroscopically following photoionization with a 200 nm laser pulse of sufficient intensity, a long progression of cluster peaks with n up to more than 40 is observed with a distribution maximum at $n \approx 8$, as illustrated in figure 7*b*. When a 4:1 Ar:ND_3 mixture is expanded at a backing pressure of 2 bar, only the lowest clusters with $n < 5$ are observed in the mass spectra (see figure 7*a*). The actual distribution of cluster sizes is likely to be shifted to higher sizes than apparent in figure 7 because the ionization of the clusters can be accompanied by evaporation of several ND_3 units.

To form ND_4 radicals we use the expansion conditions corresponding to figure 7*a*. Under these conditions, the production of unwanted ions from higher clusters can be avoided resulting in two advantages: (1) the total number of ions in the photoexcitation volume is reduced; and (2) the ion concentration can be evaluated more accurately. Indeed, at the high masses corresponding to the highest clusters in figure 7*b*, it was impossible to verify that the ion collection efficiency and the MCP detection efficiency were sufficiently close to unity to ensure a meaningful determination of ion concentrations.

The photodissociation and photoionization of $(ND_3)_n$ clusters by light pulses of ≈ 200 nm has been studied extensively in the past years (Fuke *et al.* 1994; Mizaizu *et al.* 1993; Wei *et al.* 1993; Snyder *et al.* 1996; Freudenberg *et al.* 1996). Two main mechanisms have been established as sources of ammoniated ammonium radicals and ions. The former mechanism, equations (5.1)–(5.2), consists of a two-photon ionization via the cluster equivalent of the $\tilde{A}$ state of ammonia, followed by an ion reaction producing the $(ND_3)_m(ND_4)^+$ cluster ions,

$$(ND_3)_n + h\nu \rightarrow (ND_3)_n^*, \quad (ND_3)_n^* + h\nu \rightarrow (ND_3)_n^+, \tag{5.1}$$

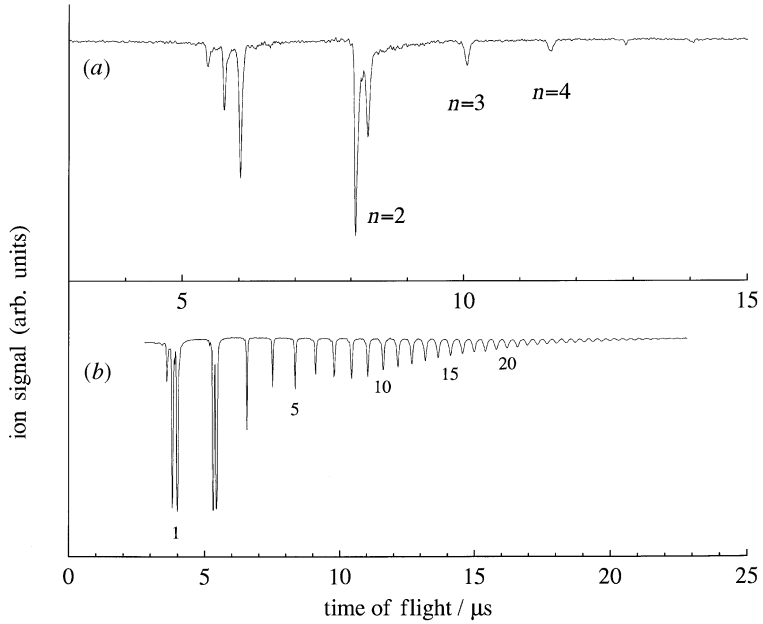

Figure 7. Ion time-of-flight spectra following photoexcitation ($\lambda = 200$ nm) of $(ND_3)_n$ clusters via the $\tilde{A}$ state of ammonia (or its cluster equivalent). The gas sample is a skimmed supersonic expansion of 6 bar of pure ND_3 for trace (b) and of 2 bar of a 4:1 Ar:ND_3 mixture for trace (a).

$$(ND_3)_n^+ \rightarrow (ND_3)_{n-2}(ND_4)^+ + ND_2. \tag{5.2}$$

This process becomes dominant at high laser fluences when the absorption of a second photon in equation (5.1) can compete with the dissociation of the $(ND_3)_n^*$ excited clusters, and is negligible, at the low laser fluences used in this study, for all clusters that have a rapidly dissociating intermediate state.

The second mechanism, equations (5.3)–(5.5), involves the absorption of a photon to the dissociative state of the cluster followed by its dissociation into ammoniated ammonium radicals. Absorption of a subsequent photon can lead to the ionization of the ammoniated ammonium radicals formed.

$$(ND_3)_n + h\nu \rightarrow (ND_3)_n^*, \tag{5.3}$$

$$(ND_3)_n^* \rightarrow (ND_3)_{n-2}(ND_4) + ND_2. \tag{5.4}$$

$$(ND_3)_{n-2}(ND_4) + h\nu \rightarrow (ND_3)_{n-2}(ND_4)^+. \tag{5.5}$$

All processes can be accompanied by a loss of ND_3 units.

At the low fluences used to produce the ammonium radical clusters (unfocused 200 nm laser light pulses of 200–300 μJ pulse^{-1} energy, 3–4 ns pulse length and 3–4 mm spot size) the mass spectra of figure 7 are dominated by ammoniated ammonium ions formed by the second mechanism. At the lower masses ND_2^+, ND_3^+ and $(ND_3)_2^+$ peaks can also be seen but $(ND_3)_n^+$ ion peaks with $n > 2$ are almost completely absent from the mass spectra. They can be seen as very weak peaks on the low time-of-flight side of the main $(ND_3)_{n-2}(ND_4)^+$ peaks in figure 7*b*. The occurrence of a surprisingly strong $(ND_3)_2^+$ peak in the mass spectra of figure 7 has been observed in previous studies and has been attributed to the special features of the dynamics of the excited dimer state (Freudenberg *et al.* 1996).

At sufficiently low fluences of the photodissociation laser, the ionization of the

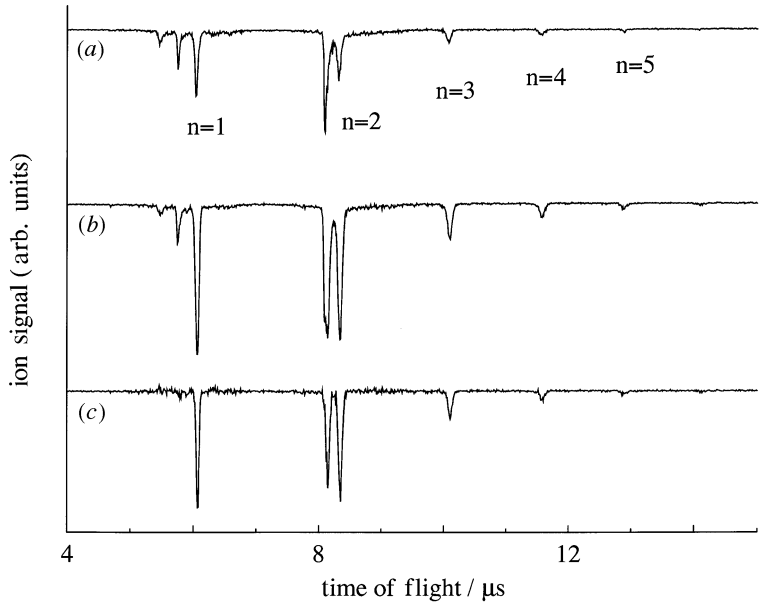

Figure 8. Ion time-of-flight spectra following photoexcitation ($\lambda = 200$ nm) of $(ND_3)_n$ clusters via the $\tilde{A}$ state of ammonia (or its cluster equivalent). The gas sample is a skimmed supersonic expansion of 2 bar of a 4:1 Ar:ND_3 gas mixture. Trace (*a*) was recorded with only the 200 nm laser beam. Trace (*b*) was obtained with a 260 nm laser applied 28 ns after the 200 nm laser. Trace (*c*) is the difference between trace (*b*) and (*a*) and represents the ions produced by the second laser only.

ammonium radicals in process (5.5) becomes less efficient and ammonium radicals, provided that they are sufficiently long lived, remain available for spectroscopic investigations with a second delayed laser. Traces (*a*)–(*c*) in figure 8 illustrate the effect of probing the ammoniated ammonium cluster beam with a second laser ($\lambda = 265$ nm) delayed by 28 ns with respect to the photodissociation laser. Traces (*a*) and (*b*) in figure 8 show the distribution of ions produced by the first laser only (equations (5.3)–(5.5)), and by both lasers, respectively. The lower trace shows the difference between trace (*b*) and trace (*a*) and corresponds to the ions that have been produced by the second delayed laser alone. The second laser clearly contributes to form ammoniated ammonium ions and $(ND_3)_2^+$ ions but does not contribute to form ND_2^+ or ND_3^+ ions. The enhancement of all ammoniated ammonium ion peaks by the second delayed laser demonstrates that the radicals, and in particular the ammonium radical, are produced in sufficient quantity for spectroscopic investigation to be carried out under our experimental conditions.

Integrating the total ion signal in the second mass spectrum (trace (*b*)) in figure 8 leads to an estimate of the ion concentration in our experiment. Approximately 500 ions are produced per laser shot in an ionization volume of approximately 0.05 cm^3, leading to ion concentrations of 10^4 ions cm^{-3}. At these low ion concentrations, no recurrent field ionization could be observed in experiments with pulsed sequences such as those described in § 4. The best resolution achieved in the PFI–ZEKE spectrum of the ND_4 radical under these conditions amounts to 0.6 cm^{-1} (see later), which is sufficient to resolve the rotational structure, but is a factor of three broader than the resolution achieved in the PFI–ZEKE spectrum of NO presented in figure 6. The lower resolution of the ZEKE spectrum is not limited by the laser linewidth

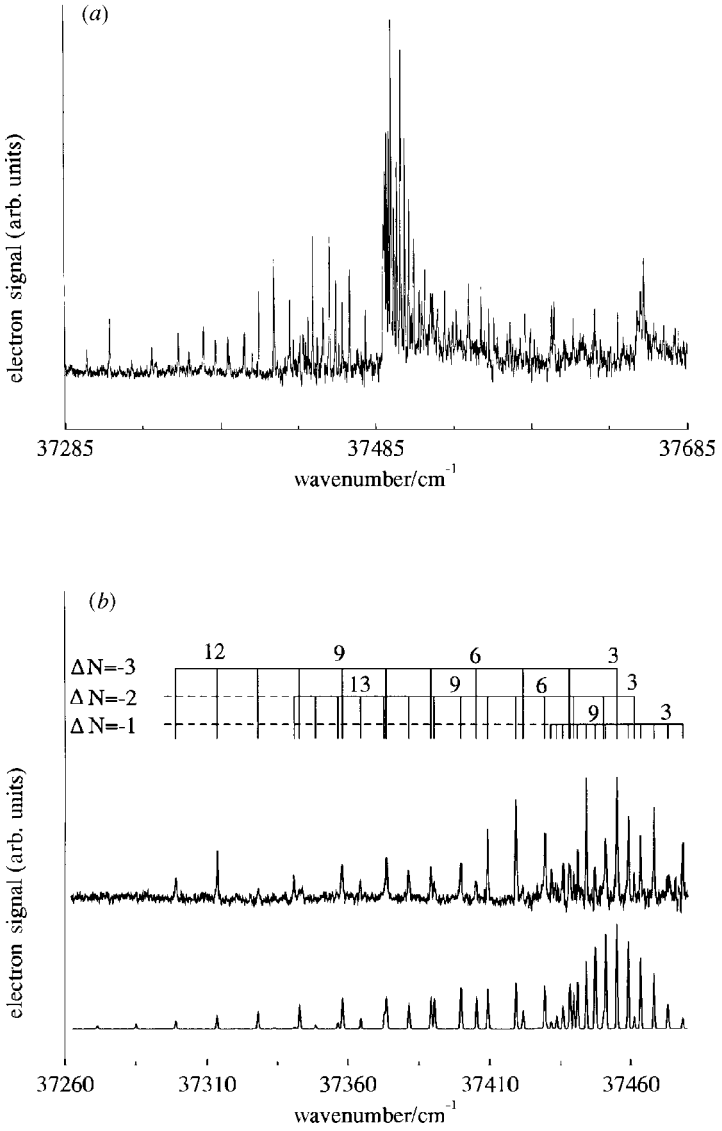

Figure 9. (*a*) Overall PFI–ZEKE spectrum of the ND_4^+ $\tilde{X}$ $^1A_1 \leftarrow ND_4$ 3s $^2A_1$ transition. (*b*) Detail of the rotational structure (upper trace) with a simulated spectrum (lower trace). The transitions are labeled by the total angular momentum quantum number N (neglecting spin) in the ground neutral state and are grouped according to the value of $\Delta N = N^+ - N$.

(better than $0.2\,cm^{-1}$) nor by the pulsed field ionization (the pulsed sequence used in the recording of figure 6 also yielded a resolution of $0.6\,cm^{-1}$ in ND_4), but by the Doppler effect. The ND_4 radicals are produced in a cluster dissociation process and their velocity distribution is not as cold as that of other particles in the supersonic beam. Because our expansion conditions favour the formation of small clusters (see figures 7*a* and 8), a rough estimate of the maximum amount of kinetic energy released in equation (5.4) can be obtained from the thermodynamics of the corresponding dimer reactions. Translationally colder distributions are expected if the ND_4 formation is accompanied by a loss of many ND_3 units and/or if the ND_2

fragment is produced with high internal energy. The maximum kinetic energy release $E_{k\,\max}$, corresponding to production of ND_4 and ND_2 radicals in their lowest rovibronic states, can be obtained from

$$\tilde{\nu}_{\rm diss} = D_0(ND_3 - ND_3) + D_0(ND_2 - D) - D_0(ND_3 - D) + E_{k\,\max}. \tag{5.6}$$

With $\tilde{\nu}_{\rm diss} = 49\,430\ {\rm cm}^{-1}$, and values of $970\ {\rm cm}^{-1}$ for $D_0(ND_3 - ND_3)$ (Kamke *et al.* 1988), of $38\,010\ {\rm cm}^{-1}$ for $D_0(ND_2 - D)$ (Mordaunt *et al.* 1996) and of $-250\ {\rm cm}^{-1}$ for $D_0(ND_3 - D)$ (Gellene *et al.* 1982), $E_{k\,\max}$ is estimated to be approximately $10\,000\ {\rm cm}^{-1}$, which would be consistent with a Doppler broadening of $0.6\ {\rm cm}^{-1}$.

Figure 9*a* shows the overall PFI–ZEKE spectrum of the photoelectronic transition between the vibrationless 3s $^2A_1$ ground neutral state of ND_4 and the $\tilde{X}\ ^1A_1$ ground vibronic state of the ND_4^+ ion, and a part of its assigned rotational structure is displayed in figure 9*b* with a simulated spectrum. The spectrum is rotationally resolved and the detailed analysis of the rotational structure of the spectrum, including a discussion of the observed propensity rules for photoionization in this tetrahedral molecule, has been presented elsewhere (Signorell *et al.* 1997). Only the main results are summarized here. The line positions can be fitted according to

$$\tilde{\nu}_{N,N^+} = \tilde{\nu}_{00} + B_0^+ N^+(N^+ + 1) - D_0^+(N^+(N^+ + 1))^2 - [B_0 N(N+1) - D_0(N(N+1))^2], \tag{5.7}$$

which corresponds to energy differences between the rotational levels of two vibronic states of A_1 symmetry in a tetrahedral (spherical top) molecule. The fit leads to the determination of an ionization potential of $37\,490.7 \pm 1.5\ {\rm cm}^{-1}$, and of rotational and centrifugal distortion constants for the neutral state ($B_0 = 2.8560 \pm 0.0037\ {\rm cm}^{-1}$ and $D_0 = (4.78 \pm 1.4) \times 10^{-5}\ {\rm cm}^{-1}$) and for the ionic state ($B_0^+ = 2.9855 \pm 0.0037\ {\rm cm}^{-1}$ and $D_0^+ = (4.77 \pm 1.5) \times 10^{-5}\ {\rm cm}^{-1}$). The propensity for core rotational angular momentum changes following photoionization are $\Delta N = 0$, ± 1, ± 2 and ± 3. The observed transitions are between neutral levels of rovibronic symmetry $(A_1; A_2; E; F_1; F_2)$ and ionic levels of rovibronic symmetry $(A_1, A_2; A_1, A_2; E; F_1, F_2; F_1, F_2)$, respectively. Further details concerning the implications of these observed photoionization selection and propensity rules on the photoionization of tetrahedral molecules and on the threshold photoionization dynamics of the ammonium radical are discussed in Signorell *et al.* (1997). The determination of the rotational constant of the ammonium radical demonstrates that PFI–ZEKE spectroscopy is not only useful to derive spectroscopic information on ions, but also on neutral molecules.

6. Conclusions

We have demonstrated:

(i) that ions produced in the vicinity of high Rydberg states not only enhance their stability with respect to decay processes such as autoionization and predissociation, but also modify their field ionization behaviour;

(ii) that sequences of pulsed electric fields of equal magnitude are a sensitive probe of the interaction between ions and high Rydberg states;

(iii) that a correlation exists between the minimum electric field required to inhibit a recurrent pulsed field ionization signal and the ion concentration;

(iv) that this correlation may be used to obtain a rough estimate of the ion concentration in a PFI experiment on high Rydberg states;

(v) that ion concentrations have to be reduced to below $10^4\ {\rm ions\,cm}^{-3}$ for the

effects of ions on the pulsed field ionization behaviour of high Rydberg states in the range $100 < n < 350$ to become negligible; and

(vi) that the resolution achievable by PFI–ZEKE photoelectron spectroscopy can be improved to significantly better than 1 cm^{-1} under conditions where ion concentrations have been minimized.

We thank R. Gunziger and H. Schmutz for their help in the development of the experimental setup.

References

Alberti, F., Huber, K. P. & Watson, J. K. G. 1984 Absorption spectrum and analysis of the ND_4 Schüler band. *J. Mol. Spectrosc.* **107**, 133–143.

Alt, C., Scherzer, W. G., Selzle, H. L. & Schlag, E. W. 1995*a* Intensity and lifetimes of ZEKE spectra. *Chem. Phys. Lett.* **240**, 457–460.

Alt, C. E., Scherzer, W. G., Selzle, H. L., Schlag, E. W., Baranov, L. Ya. & Levine, R. D. 1995*b* How large are high molecular Rydberg states? A direct experimental test. *J. Phys. Chem.* **99**, 1660–1665.

Bethe, H. A. & Salpeter, E. E. 1957 *Quantum mechanics of one- and two-electron atoms*. Berlin: Springer.

Chupka, W. A. 1993 Factors affecting lifetimes and resolution of Rydberg states observed in zero-electron-kinetic-energy spectroscopy. *J. Chem. Phys.* **98**, 4520–4530.

Dietrich, H.-J., Müller-Dethlefs, K. & Baranov, L. Ya. 1996 Fractional Stark state selective electric field ionization of very high-n Rydberg states of molecules. *Phys. Rev. Lett.* **76**, 3530–3533.

Freudenberg, T., Radloff, W., Ritze, H.-H., Stert, V., Weyers, K., Noack, F. & Hertel, I. V. 1996 Ultrafast fragmentation and ionization dynamics of ammonia clusters. *Z. Phys.* D **36**, 349–364.

Fuke, K., Takasu, R. & Mizaizu, F. 1994 Photoionization of hypervalent molecular clusters: electronic structure and stability of $NH_4(NH_3)_n$. *Chem. Phys. Lett.* **229**, 597–603.

Gallagher, T. F. 1994 *Rydberg atoms*. Cambridge University Press.

Gellene, G. I., Cleary, D. A. & Porter, R. F. 1982 Stability of the ammonium and the methylammonium radicals from neutralised ion-beam spectroscopy. *J. Chem. Phys.* **77**, 3471–3477.

Herzberg, G. 1981 Rydberg spectra of triatomic hydrogen and of the ammonium radical. *Faraday Disc. Chem. Soc.* **71**, 165–173.

Holtsmark, J. 1919 Über die Verbreiterung von Spektrallinien. *Annln Phys.* **58**, 577–630.

Hsu, C.-W., Lu, K. T., Evans, M., Chen, Y. J., Ng, C. Y. & Heimann, P. 1996 A high resolution photoionization study of Ne and Ar: observation of mass analysed threshold ions using synchrotron radiation and direct current electric fields. *J. Chem. Phys.* **105**, 3950–3961.

Huber, K. P. & Sears, T. J. 1985 Emission spectra in a supersonic expansion: the quartet system of NO and the Schüler band of ND_4. *Chem. Phys. Lett.* **113**, 129–134.

Jortner, J. & Bixon, M. 1995 On the dynamics of high Rydberg states of large molecules. *J. Chem. Phys.* **102**, 5636–5646.

Jungen, Ch. & Miescher, E. 1969 Absorption spectrum of the NO molecule. IX. The structure of the f complexes, the ionization potential of NO, and the quadrupole moment of NO^+. *Can. J. Phys.* **47**, 1769–1787.

Kamke, W., Herrmann, R., Wang, Z. & Hertel, I. V. 1988 On the photoionization and fragmentation of ammonia clusters using TPEPICO. *Z. Phys.* D **10**, 491–497. (This value is valid for the ammonia dimer and we make the approximation here that it is also valid for $(ND_3)_2$, an approximation that is likely to slightly underestimate the binding energy.)

Merkt, F. 1994 Collisional and electric field effects in the delayed pulsed field ionization zero-kinetic-energy photoelectron spectrum of argon. *J. Chem. Phys.* **100**, 2623–2628.

Merkt, F. & Softley, T. P. 1992*a* Final-state interactions in the zero-kinetic-energy-photoelectron spectrum of H_2. *J. Chem. Phys.* **96**, 4149–4156.

Merkt, F. & Softley, T. P. 1992*b* Rotationally resolved zero-kinetic-energy photoelectron spectrum of nitrogen. *Phys. Rev.* A **46**, 302–314.

Merkt, F. & Softley, T. P. 1993 Rotational line intensities in zero kinetic energy photoelectron spectroscopy (ZEKE–PES). *Int. Rev. Phys. Chem.* **12**, 205–239.

Merkt, F. & Zare, R. N. 1994 On the lifetimes of Rydberg states probed by delayed pulsed field ionization. *J. Chem. Phys.* **101**, 3495–3505.

Merkt, F., Mackenzie, S. R. & Softley, T. P. 1995 Rotational autoionization dynamics in high Rydberg states of nitrogen *J. Chem. Phys.* **103**, 4509–4518.

Merkt, F., Rednall, R. J., Mackenzie, S. R. & Softley, T. P. 1996 Electric field ionization of high Rydberg states of Ar with sequences of identical pulses. *Phys. Rev. Lett.* **76**, 3526–3529.

Miescher, E. 1976 High resolution absorption spectrum of nitric oxide (NO) in the region of the first ionization limit. *Can. J. Phys.* **54**, 2074–2092.

Miescher, E. & Huber, K. P. 1976 Electronic spectrum of the NO molecule. In *International review of science* (ed. D. A. Ramsay), Physical Chemistry Series 2, vol. 3 pp. 37–73. London: Butterworths.

Mizaizu, F., Houston, P. L., Nishi, N., Shinohara, H., Kondow, T. & Kinoshita, M. 1993 Formation of protonated ammonia cluster ions: two-color two-photon ionization study. *J. Chem. Phys.* **98**, 336–341.

Mordaunt, D. H., Dixon, R. N. & Ashfold, M. N. R. 1996 Photodissociation dynamics of $\tilde{A}$ state ammonia molecules. II. The isotopic dependence of partially and fully deuterated isotopomers. *J. Chem. Phys.* **104**, 6472–6481.

Muhlpfordt, A. & Even, U. 1995 Autoionizing Rydberg and zero electron kinetic energy states in Ar. *J. Chem. Phys.* **103**, 4427–4430.

Palm, H. & Merkt, F. 1997 Ion density effects in the pulsed field ionization of high Rydberg states. *Chem. Phys. Lett.* (In the press.)

Pratt, S. T. 1993 Electric field effects in the near-threshold photoionization spectrum of nitric oxide. *J. Chem. Phys.* **98**, 9241–9250.

Reiser, G., Habenicht, W., Müller-Dethlefs, K. & Schlag, E. 1988 The ionization energy of nitric oxide. *Chem. Phys. Lett.* **152**, 119–123.

Remacle, F. & Levine, R. D. 1996 Rotational autoionization and interseries coupling of high Rydberg states by the anisotropy of the molecular core: the quantal long time evolution. *J. Chem. Phys.* **105**, 4649–4663.

Schüler, H., Michel, A. & Grün, A. E. 1955 Über neue Emissionsbanden bei elektrischer Anregung des Ammoniaks. *Z. Naturf.* A **10**, 1–2.

Signorell, R., Palm, H. & Merkt, F. 1997 Structure of the ammonium radical from a rotationally resolved photoelectron spectrum. *J. Chem. Phys.* **106**, 6523–6533.

Smith, J. M. & Chupka, W. A. 1995 Electron transfer in high-n Rydberg states *J. Chem. Phys.* **103**, 3436–3439.

Snyder, E. M., Purnell, J., Wei, S., Buzza, S. A. & Castleman Jr, A. W. 1996 Real-time dynamics of ammonia clusters excited through the $\tilde{A}$ state: formation of the protonated cluster ions. *Chem. Phys.* **207**, 355–366.

Vrakking, M. J. J. & Lee, Y. T. 1995*a* Lifetimes of Rydberg states in zero-electron-kinetic-energy experiments. I. Electric field induced and collisional enhancement of NO predissociation lifetimes. *J. Chem. Phys.* **102**, 8818–8832.

Vrakking, M. J. J. & Lee, Y. T. 1995*b* Lifetimes of Rydberg states in zero-electron-kinetic-energy experiments. II. Electric field induced and collisional enhancement of Xe autoionization lifetimes. *J. Chem. Phys.* **102**, 8833–8841.

Vrakking, M. J. J., Fischer, I., Villeneuve, D. M. & Stolow, A. 1995 Collisional enhancement of Rydberg lifetimes observed in vibrational wave packet experiments. *J. Chem. Phys.* **103**, 4538–4550.

Watson, J. K. G. 1986 Vibration-rotation structure in the electronic spectrum of the ammonium radical. *NBS Spec. Publ.* **716**, 650–670.

Wei, S., Purnell, J., Buzza, S. A. & Castleman Jr, A. W. 1993 Ultrafast reaction dynamics of electronically excited $\tilde{A}$ state of ammonia clusters. *J. Chem. Phys.* **99**, 755–757.

Weitzel, K.-M. & Güthe, F. 1996 The distinction of direct and pulsed-field ionized zero kinetic energy photoelectrons in electron/ion coincidence experiments. *Chem. Phys. Lett.* **251**, 295–300.

Whittaker, E. A., Sullivan, B. J., Bjorklund, G. C., Wendt, H. R. & Hunziker, H. E. 1984 ND_4 Schüler band absorption observed by laser FM spectroscopy in a photochemical reaction. *J. Chem. Phys.* **80**, 961–962.

Williams, B. W. & Porter, R. F. 1980 Energetics of fragmentation of CH_5, H_3O and NH_4 from neutralised ion-beam experiments. *J. Chem. Phys.* **73**, 5598–5604.

Zhang, X., Smith, J. M. & Knee, J. L. 1993 Dynamics of high-n molecular Rydberg states with application to mass analysed threshold ionization spectroscopy. *J. Chem. Phys.* **99**, 3133–3136.

PHILOSOPHICAL TRANSACTIONS OF THE ROYAL SOCIETY A MATHEMATICAL, PHYSICAL & ENGINEERING SCIENCES